Applied Surface Science 531 (2020) 147232

Contents lists available at ScienceDirect

Applied Surface Science

journal homepage: www.elsevier.com/locate/apsusc

Mechanism of hydration of biocompatible silica-casein aerogels probed by NMR and SANS reveal backbone rigidity

István Lázár[a,b], Attila Forgács[a,b], Anita Horváth[a], Gábor Király[c], Gábor Nagy[c], Adél Len[d], Zoltán Dudás[d], Vanda Papp[a], Zoltán Balogh[a], Krisztián Moldován[a], Laura Juhász[e], Csaba Cserháti[e], Zsuzsanna Szántó[a], István Fábián[a,b], József Kalmár[a,b,*]

[a] Department of Inorganic and Analytical Chemistry, University of Debrecen, Egyetem tér 1, Debrecen H-4032, Hungary
[b] MTA-DE Redox and Homogeneous Catalytic Reaction Mechanisms Research Group, Egyetem tér 1, Debrecen H-4032, Hungary
[c] Department of Molecular Biotechnology and Microbiology, University of Debrecen, Debrecen H-4032, Hungary
[d] Neutron Spectroscopy Department, Centre for Energy Research, Konkoly-Thege Miklós út 29-33, Budapest H-1121, Hungary
[e] Department of Solid State Physics, University of Debrecen, Bem tér 18/b, Debrecen H-4026, Hungary

ARTICLE INFO

This article is dedicated to the loving memory of Prof. Dr. János Füzi (Wigner Research Centre for Physics).

Keywords:
Hybrid material
Aerogel
Casein
NMR spectroscopy
Hydration mechanism

ABSTRACT

Starting from TMOS and implementing co-gelation in the sol-gel method, silica was hybridized with an industrial formulation of bovine casein. The hybrid alcogels were dried in supercritical CO_2 to yield crack-free silica-casein aerogel monoliths of casein contents ranging from 4.7 wt% to 28 wt%. Cross-linked hybrid aerogels were produced from formaldehyde treated alcogels. The microstructures and the morphologies of the silica-casein aerogels highly resemble to that of pristine silica aerogels. The primary building blocks are spherical particles that interconnect into mesoporous networks (average d_{pore} = 20 nm and S_{BET} = 700 nm^2/g), as shown by SEM, small-angle neutron scattering (SANS) and N_2 adsorption-desorption porosimetry. Contrast variation SANS experiments show that silica and casein form homogeneous nanocomposite backbones. The interaction of water with silica-casein aerogels was investigated by SANS, and by NMR cryoporometry, relaxometry and diffusiometry. Even when fully saturated with water, the hybrid silica-casein aerogels retain their original, highly permeable, open mesoporous structures that formed under supercritical drying. This represents a unique and advantageous wetting mechanism among hybrid inorganic-biopolymer materials, since the strong hydration of the biopolymer component often causes the deformation of the backbone and the consequent collapse of the porous structure. Silica-casein aerogels are biocompatible and inert for CHO-K1 cells.

1. Introduction

Supercritically dried, mesoporous aerogels made of biological macromolecules (polysaccharides, proteins) are versatile advanced materials. Their key macroscopic properties (high specific surface area, low thermal conductivity, low density, high compressive strength) are the direct consequence of their microscopic structural features, such as the high strength of their backbones, their high porosities and open porous structures. Relying on these characteristics, the main research directions for the applications of biopolymer based aerogels are as follows: *i*) thermal and electrical insulation for industrial applications; *ii*) high performance adsorbents for gas separation and for environmental remediation; *iii*) catalysts and catalyst supports; *iv*) drug delivery systems, and scaffolds for tissue engineering and regenerative medicine [1–8].

One strategy to obtain novel functional aerogels is via the hybridization of biological macromolecules with silica. The most frequently used biopolymers are proteins and carbohydrate polymers [2,9–17]. The incorporation of silica into the backbones of biopolymer aerogels dramatically alter both the physical and the chemical properties of the matrices, ultimately leading to new properties that often significantly differ from those of the pristine components [10–12,18–24]. The hybridization of silica with starch, gelatin, alginate, chitosan and silk fibroin have been explored in previous studies. Many hybrids have been tested in drug delivery applications and as adsorbents for hazardous materials [2,6,7,12,20,21,25–29]. The biocompatibility and the biodegradability of these hybrids are superior compared to silica. In general, the molecular level structural features of the hybrid aerogels directly determine their application related properties.

* Corresponding author at: Department of Inorganic and Analytical Chemistry, University of Debrecen, Egyetem tér 1, Debrecen H-4032, Hungary.
E-mail address: kalmar.jozsef@science.unideb.hu (J. Kalmár).

https://doi.org/10.1016/j.apsusc.2020.147232
Received 25 March 2020; Received in revised form 20 June 2020; Accepted 9 July 2020
Available online 21 July 2020

Casein is a naturally abundant protein with potential applications in polymer chemistry. It can be incorporated into polymer networks via well-controlled ways, which usually result in the enhanced rigidity and functionality of the matrix [30–34]. However, porous silica-casein hybrid materials have scarcely been reported.

When aerogels are designed to be used in aqueous media, e.g. in biomedical or environmental engineering applications, it is essential to understand the mechanism of their hydration and the consequent changes in the aerogel structure. The most important questions are the following. 1) Does the extensive hydration of the backbone cause the erosion of the aerogel monolith? 2) What is the stable particle size and surface charge of the hydrated aerogel? 3) Does the aerogel retain its original morphology and pore structure when hydrated? 4) Are the pores of the aerogels permeable in water, or does the porous structure collapse due to the extensive deformation of the hydrated backbone? Evidently, the answers to these questions are indispensable to understand the properties of hydrated aerogels related to mass transport, adsorption-desorption phenomena, suspension stability and biocompatibility [35–40]. One particular characteristic of silica-biopolymer hybrid aerogels is, that the extensive hydration of the biopolymer components in water causes the distortion and the swelling of the backbone, which leads to the partial or complete collapse of the open aerogel structures [26,41,42]. The collapse of the pores leads to the decrease of the specific surface area and the hindrance of mass transport from and into the hydrated aerogel particles. Thus, designing hybrids that do not display these adverse hydration properties is in high demand.

In order to meet the above detailed requirements, we synthesized silica-casein hybrid aerogels of casein contents varying from ca. 5 wt% to 30 wt%. Some variants of the hybrids were chemically crosslinked by formaldehyde. The microscopic structures of the silica-casein aerogels were investigated by SEM, infrared spectroscopy (FT-IR), N_2 adsorption-desorption porosimetry and small-angle neutron scattering (SANS). The interaction of the silica-casein aerogels with water was also thoroughly investigated by SANS and by non-conventional NMR methods, such as cryoporometry, relaxometry and diffusiometry [43]. Aqueous particle size distribution and Zeta potentials are also reported. Finally, we discuss the mechanical properties and the biocompatibility of the new silica-casein aerogels.

2. Experimental

2.1. Materials

Tetramethyl orthosilicate (TMOS) was purchased from Sigma–Aldrich. Ammonia solution (25%) methanol and acetone were purchased from Molar Chemicals Ltd. (Hungary), and formaldehyde (37%) was from VWR International Ltd. (Hungary). Double deionized and ultrafiltered water (ρ = 18.2 MΩ cm) was prepared by a MilliQ (Millipore) equipment. Biogon-C, 99.5% carbon dioxide cylinder equipped with a dip tube was purchased from Linde Gas Ltd. (Hungary).

2.1.1. Casein formulation

The synthesis of the hybrid aerogels was realized from “MPI 85” casein powder, which was manufactured and provided by the Hungarian Dairy Research Institute Ltd. (Mosonmagyaróvár, Hungary). MPI 85 is a protein mixture, which contains 68.5% casein protein, 12.0 wt% whey protein and 19.5% non-protein constituents. The non-protein constituents are: 1.1 wt% milk fat, 6.8 wt% lactose, 6.5 wt% ash and 5.1 wt% moisture. The IR spectrum of the as-received “MPI 85” casein powder is reported in Section 3.1.2.

2.2. Synthesis of silica-casein hybrid aerogels

Three reactant solutions were prepared and designated as solution A, B and C. In solution A, the silane reagent TMOS (2.5 cm^3, 13.7 mmol) was dissolved in methanol (15 cm^3, 371 mmol). Solution B contained aqueous ammonia solution (1 cm^3, 12.1 mmol NH_3 and ca. 34 mmol water) and water (1 cm^3, 55.6 mmol) mixed with methanol (5 cm^3, 124 mmol). In solution C, different quantities of the MPI 85 casein powder were completely dispersed in water (4 cm^3, 222 mmol), as given in Table 1. For the preparation of the hybrid aerogels, solution B was added to solution A in a beaker during constant stirring. After a few minutes of mixing, solution C was also added. The sol that formed in the reaction was immediately transferred into a plastic mold. The transparent homogenous solution developed into a gel in a few minutes. The gel was kept in the mold for 3 days for completing the gelation.

Table 1
The composition of silica-casein hybrid aerogels. The recipes are given in Sections 2.1 and 2.2. The letter F denotes cross linked aerogels.

CODE	amount of casein in solution C (g)	casein content of hybrid aerogel (wt.%)	formaldehyde added during solvent exchange (cm^3)
SC5	0.050	4.7	–
SC5F	0.050	4.7	10
SC30	0.40	28	–
SC30F	0.40	28	10

Subsequently, the gel was placed into a perforated aluminum container, and solvent exchange was started. For two days, the gel was kept in methanol, for another 2 days it was in acetone:methanol 1:1 solution, and after that, it was kept in acetone for a week. The acetone was refreshed 3 times during this period. In order to remove the traces of water from the porous system, a continuous-mode solvent regeneration and extraction unit was used for 3 days with fresh acetone every day. The casein contents of the spent solvents were regularly checked. No leach of casein was detected during the multi-step solvent exchange procedure. Furthermore, there was no unreacted TMOS and no dissolved casein detected in the starting methanol phase after gelation. Thus, it is reasonable to assume that the total amount of casein is covalently incorporated into the hybrid backbone of the gel (Table 1).

Supercritical drying was performed by using the medium temperature technique, as published earlier [44]. A pumpless drying system was used, where acetone was extracted with liquid CO_2 at 5.4 MPa (room temperature), then the gel was dried with supercritical CO_2 at 14 MPa and 80 °C. Finally, depressurization is performed in minute steps [44,45].

2.3. Synthesis of crosslinked silica-casein hybrid aerogels

In the synthesis of the crosslinked hybrid aerogels, all steps were identical to the synthesis of the pristine silica-casein hybrid aerogels until the solvent exchange. The difference was that 10 cm^3 (0.134 mol) formaldehyde was added to 200 cm^3 (4.96 mol) methanol at the first step of the solvent exchange. This amount of formaldehyde is in high excess over casein. The gels were kept in the formaldehyde containing mixture for a week. This time was needed for formaldehyde to completely impregnate the wet gels through the pores by diffusion [31,33]. After this step, solvent exchange and supercritical drying were performed in the same manner as for the pristine gels. The supercritically dried pristine silica-casein aerogels developed a yellow hue, while the crosslinked aerogels remained white.

2.4. Characterization of aerogels

2.4.1. Conventional techniques

The dry, as prepared aerogels were characterized by scanning electron microscopy (SEM), infrared spectroscopy (IR) and N_2 gas adsorption-desorption porosimetry as described in the Supporting Information.

2.4.2. Compressive strength and flexibility tests

The compressibility of aerogel monoliths was measured with an Instron 4302 universal strength testing apparatus. The length of the monolithic test objects was 40 ± 7 mm, and the diameter was 25 ± 1 mm. The crosshead speed of the probe was 1.0 mm/min. Compression was limited by the operating range of the strength testing head (10 kN). Data were collected with the INSTRON Series IX Automated Materials Tester v.8.30.00 software.

Mechanical flexibility measurements were performed on a custom-built apparatus. The monolithic aerogel sample was placed on a laboratory balance and it was pressed with a probe object. The test object was a Teflon measuring cone with 1.0 mm curvature and 60° cone angle. The cone was pressed with increasing force into the aerogel, and the depth of penetration was measured with a precision ruler installed next to the monolithic aerogel sample. The measurement was continued until a maximum load of 60 g was expressed on the sample, or until the monolith cracked.

2.4.3. Small angle neutron scattering (SANS)

Dry, powdered aerogel samples were introduced into 2 mm thick quartz cuvettes and measured without any pre-treatment. Some samples were hydrated either with H_2O or with a 2:1 vol ratio H_2O – D_2O mixture (64 wt% H_2O and 36 wt% D_2O) to a water / dry aerogel mass ratio of 3.5 g/g. After homogenization, the wet samples were stored overnight at room temperature before SANS measurements.

SANS experiments were performed on the Yellow Submarine instrument at Budapest Neutron Centre. This is a pin-hole type instrument with a two-dimensional neutron detector. Two sample-to-detector distances (1.2 m and 5.4 m) and two wavelengths (4.38 Å and 10.23 Å) were used. The beam diameter was 8 mm. The samples were measured for 60 – 180 min at room temperature. By altering the wavelength and sample detector distance, a Q range of 0.008 – 0.4 $Å^{-1}$ was covered. The momentum transfer (Q) is defined by the following equation:

$$Q = \frac{4\pi}{\lambda}\sin\frac{\theta}{2} \tag{1}$$

where λ is the wavelength of the monochromatic neutron beam and Θ is the scattering angle. The definition of the scattering intensity (I) is as follows:

$$I(\lambda, \theta) = I_0(\lambda)\Delta\Omega\eta(\lambda)TV\frac{d\Sigma}{d\Omega}(Q) \tag{2}$$

where λ is the wavelength of the monochromatic neutron beam, Θ is the scattering angle, I_0 is the incoming neutron flux, ΔΩ is the unit solid angle, $\eta(\lambda)$ is the detector efficiency, $T$and V are the transmission and volume of the sample and $\frac{d\Sigma}{d\Omega}(Q)$ is the macroscopic differential cross section. The macroscopic differential cross section conveys structural information on the studied system. The measured scattering intensity was corrected for sample transmission, empty cell scattering, solvent scattering, detector sensitivity and background scattering. The nano- and microstructural parameters of the scattering objects are determined from the mathematical analysis of the corrected $I(Q)$ curves.

For silica and silica based aerogels that show a wide variety of fractal scaling, a unified approach (described by Beaucage) can be used, covering the whole Q range [46,47].

$$I(Q) \cong A\exp\left(-\frac{Q^2Rg^2}{3}\right) + B\left\{\frac{\left[\operatorname{erf}\left(\frac{QRg}{\sqrt{6}}\right)\right]^3}{Q}\right\}^{-p} \tag{3}$$

Rg is the average gyration radius, p is the power law exponent (called Porod exponent, when its value is exactly 4), and A and B are coefficients related to the volume and number density of the scattering objects and to their contrast. Parameters A and B can be treated as adjustable scaling parameters.

Data fitting was performed by using the built-in least-squares algorithms of the Igor Pro 6.1 software [48].

2.4.4. Particle size of wet aerogels

The size distribution of aerogel particles was measured by using a hemocytometer and image analysis after wet grinding the samples by a Potter-Elvehjem tissue grinder (10 min) and sonication (5 min). Images were taken from c = 0.5 mg/mL suspensions with a 1.3 MP USB microscope camera. The ImageJ software was used for calculating the size distribution of the particles.

2.4.5. Zeta potential of aerogel particles

Aerogels were wet ground by a tissue grinder (see above), and the zeta potential was measured at a final aerogel concentration of 0.1 mg/mL on a MALVERN Zetasizer Nano ZS instrument using conventional instrument setup and operation.

2.4.6. NMR relaxometry

NMR relaxometry measurements were performed with a Minispec Bruker mq20 relaxometer instrument. Approximately 50 mg dry aerogel was weighed into an NMR tube, and it was titrated with water. The water / dry aerogel mass ratio was increased up to 3.5 g/g in 12 – 15 steps [49–51]. The wet aerogel samples were mixed and sonicated, and every sample was equilibrated for 24 h before the measurement. All measurements were performed at 6 dB. The T_1 (spin–lattice) and the T_2 (spin–spin) relaxation times were determined for every samples. The CPMG (Carr-Purcell-Meiboom-Gill) sequence was used with 3 different echo times (0.08 ms, 0.12 ms, and 0.16 ms) for all T_2 measurements. The parameters of the CPMG sequence were optimized according to the T_1 relaxation times determined previously using the inversion–recovery method.

The relaxation time of water is influenced by its chemical surroundings in the porous sample, i.e. water can be found in different relaxation domains in wet aerogels. Multiple T_2 values combine in the final signal if the exchange of the water molecules is slow between the different domains [52,53]. The number of exponential functions in the primary CPMG decays were determined by inverse Laplace transformation using the MERA (Multi–Exponential Relaxation Analysis) algorithm on the basis of the CONTIN method in MatLab v.8.5 (MathWorks Inc., USA).

2.4.7. NMR cryoporometry

Water was used as a probe liquid for cryoporometry. Approximately 50 mg of dry, powdered aerogel was weighed into a plastic NMR tube and ca. 250 μL water was added in order to fully saturate the pores of the aerogel. Thus, the water content (water / dry aerogel mass ratio) of the samples was ca. 5.0 g / g. After manual homogenization, the samples were sonicated and kept at + 4 °C for 24 h. NMR cryoporometry measurements were performed in a Bruker Avance II 360 MHz NMR instrument. Cooling was achieved with dried air supplied by BCU-05 and BSCU-05 cooling units.

The Carr-Purcell-Meiboom-Gill (CPMG) spin-echo pulse sequence was applied to eliminate the broad signal of the solid phase during the echo time. The remaining signal intensity is proportional to the amount of liquid water inside the pores, which changes gradually with temperature, as water freezes or ice melts. The melting and freezing points of liquids confined in nanometer wide spaces are lowered as given by the modified Gibbs-Thompson equations:

$$\Delta T_{m/f} = T_{m/f} - T_0 = -\frac{n_{m/f}K_c}{r_p} \tag{4}$$

Here, $\Delta T_{m/f}$ is the melting/freezing point depression expressed as the difference between the bulk (T_0) and confined liquid ($T_{m/f}$) phase transition temperatures. K_c is the cryoporometric constant of water, $n_{m/f}$ is a geometric factor and r_p is the pore size [54–56].

Before every measurement the 90° pulse was determined (ca.

10.7 μs). The optimal echo time was ca. 0.8 ms in order to filter the fast relaxing signal of the solid phase. Every sample was mixed with the proper amount of water and the mixture was frozen at –20 °C. Multiple melting-freezing cycles were measured between –15 °C and + 6 °C in 0.5 °C steps. Temperature was calibrated using glycol and methanol [57]. The sample was left for 5 min at a given temperature for equilibration before running the CPMG sequence. MestReNova 9.0 software was used for transforming the spectra. The measured water peak integrals were plotted against the temperature. Intensity versus temperature data was transformed to intensity versus pore size data by using the modified Gibbs-Thompson equations (eq. (4)). The numerical derivation of these yields pore size distribution plots.

2.4.8. NMR diffusiometry

The self-diffusion of water was studied in wet silica-casein hybrid aerogels at 298 K at different water / dry aerogel mass ratios. Approximately 70 mg dry aerogel was weighed into a glass NMR tube and water was added to reach ca. 0.5 g/g, 1.5 g/g and 3.5 g/g water contents. The wet aerogels were mixed, sonicated, compacted by hand and stored at room temperature for 24 h before NMR measurements. The observation time of the diffusion experiments (Δ) was varied between 10 and 140 ms. The length of the gradient pulse (δ) changed from 2 to 4 ms. A stimulated spin echo pulse sequence was used for the measurements containing bipolar gradient pulses (BIPLED) to decrease eddy currents [58,59]. The pulsed gradient strength (G) increased in 64 square distant steps from 0 to 50 G/cm. The spectra were transformed with MestReNova 9.0 software. The diffusion data were evaluated according to the general expression: [60,61]

$$I = I_0 \exp\{-D_{obs}\gamma^2(\Delta - \delta/3)\delta^2 G^2\} \quad (5)$$

When multiple diffusion domains are present in the sample, each domain is represented by a different single-exponential function of a given D_{obs} according to eq. 5, and the observed decay is the sum of these functions. If the exchange of water is slow between these domains, the different D_{obs} values can be separated [62–64]. In order to determine the number of diffusion domains, primary data were transformed by inverse Laplace transformation using the same algorithms as for the evaluation of NMR relaxometry data.

2.5. In vitro biological experiments

Chinese hamster ovary CHO-K1 cell line was used for the *in vitro* biocompatibility testing of the hybrid aerogels. Cell viability was measured by using the MTT assay. Time-lapse NIR microscopy imaging was performed in a custom-built system [25,27].

The CHO-K1 cell line is widely used for recombinant (mainly therapeutic) protein production in pharmaceutical industry. CHO cells can be genetically modified and grown either as adherent cells or in suspension. In the present study, CHO-K1 cells were grown in Ham's F12 medium supplemented with 1.25% L-glutamine 23 mM $NaHCO_3$, 100 U/ml penicillin, 100 U/ml streptomycin, 1% non-essential amino acids and 10% fetal bovine serum.

The silica-casein aerogel monoliths were ground and sieved ($d_{particle} < 250$ μm) for the *in vitro* studies. The aerogel particles were sterilized with UV light overnight before the experiments. This was realized by placing the powdered samples in UV transparent plastic containers and irradiating them in constant 360°. After sterilization, the aerogels were placed into cell free Ham's F12 medium for conditioning for 3 h, then the cells were added to the cell culture flasks. By using this methodology, no contamination of the samples was observed during the subsequent time-lapse imaging experiments.

2.5.1. MTT cell viability assay

The effect of the silica–casein aerogel microparticles on the viability of CHO-K1 cells was tested with MTT assay. The aerogel particles were added in 3 concentrations (0.2, 0.5 and 1.0 mg/ml) to the cell cultures in 96-well plates for 48 h. Untreated cells were used as control. Tests were conducted with 10.000 cells/well. After incubation, MTT (Sigma Aldrich) solution (0.5 mg/mL in PBS) 100 μL was added to each well. The plates were incubated with the reagent for 2 h at 37 °C, the wells were aspirated, and MTT formazan was extracted with 100 μL of DMSO aided by gentle agitation on a shaker. After keeping the plates at room temperature for 10 min, the absorbances were read at 570 nm by an automatic plate reader (WALLAC Victor 2 1420 spectrophotometer). The instrument blank was recorded on a row of wells to which cells had not been added. Percentage viability (respiratory competence) of the cells in each well was expressed as:

$$(Absorbance\ of\ treated\ cells / Absorbance\ of\ control\ cells) \times 100\% \quad (6)$$

Standard deviation was calculated as a measure of dispersion of data from its mean (± SD), and statistical significance is estimated by the *t*-test and one-way analysis of variance (ANOVA). *p < 0.05 is considered statistically significant and **p < 0.01 is statistically highly significant.

2.5.2. Time-lapse video imaging experiments

Modified and inverted upright microscopes (Olympus, Tokyo, Japan) were used in a SANYOMCO18-AC (Wood Dale, USA) CO_2 incubator. The cell cultures were grown to ca. 40% confluence, then the cells were treated with the aerogel microparticles (1.0 mg/ml) for 48 h. The image sequences were converted from color (24-bit red, green, and blue (RGB)) .bmp files to 8-bit grayscale .bmp files using ImageJ software. Images were acquired at 1600 × 1200 pixels with a 0.507 μm/pixel spatial resolution. For manual tracking, the MtrackJ and the Chemotaxis tool plugins were used in ImageJ software. After obtaining a series of x and y positions of separate cells, the path length and the velocity were determined. The corresponding multimedia video files are given as Supporting Information.

3. Results and discussion

For the sake of simplicity, silica-casein aerogels of different composition are referred to by using short codes as given in Table 1. SC5 stands for the pristine aerogel of 4.7 wt% casein content and SC30 stands for the pristine aerogel of 28 wt% casein content. The codes that finish with letter F denote aerogels treated with the crosslinking agent formaldehyde.

3.1. Characterization of dry aerogels

3.1.1. Scanning electron microscopy (SEM)

Representative images of pristine and crosslinked silica-casein aerogels are shown in Fig. 1. The backbones of all hybrid aerogels are built from small primary globules of $d_{globule} = 15 – 20$ nm. Most of the pores visible in the fresh fracture surfaces are in the mesopore range. A few macropores are also present, mainly in the aerogels of higher casein content (SC30 and SC30F). Altogether, the key morphological features of the hybrid aerogels are almost identical to those of the parent silica aerogels [65]. A minor morphological difference can be detected between the hybrids of low and high casein contents. In the case of the 30 wt% casein aerogels, the primary globules occasionally form densely packed ridges, but the appearance of these ridges is scarce.

The formation of globules is typical in the sol-gel synthesis of silica and silica based hybrid aerogels. The first steps of the hydrolysis and polycondensation of the TMOS silica precursor yield primary particles. Subsequently, these particles increase in size and aggregate with each other to finally yield a self-sustaining gel network. The highly similar morphologies of silica and silica-casein aerogels suggest that casein does not interfere in the primary reactions leading to the formation of the gel network, and thus, most probably hybridizes with silica at the nanometer level. The homogeneity of the hybrid backbone is discussed further in connection with SANS measurements in Section 3.4.2.

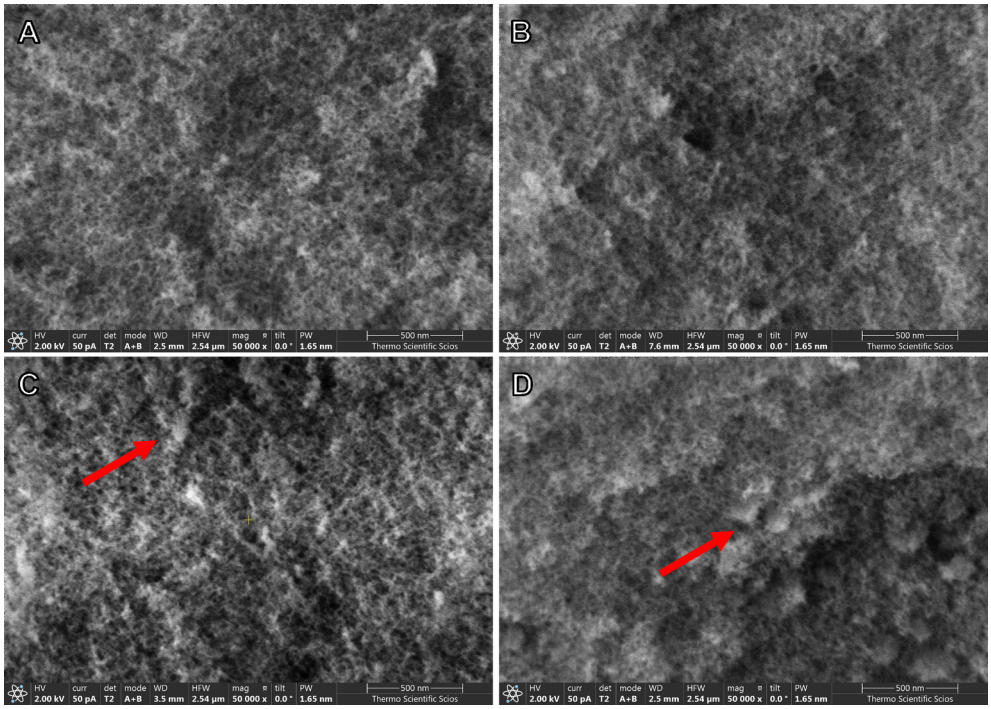

Fig. 1. SEM images of silica-casein hybrid aerogels A: SC5, B: SC5F, C: SC30, D: SC30F. The red arrows point to ridges in the structures. Magnification is × 50 k, and the scale bar shows 500 nm. (For interpretation of the references to color in this figure legend, the reader is referred to the web version of this article.)

The reaction of silica-casein with formaldehyde does not alter the morphological features of the hybrid aerogels, as seen by comparing the SEM images of the analogous pristine and crosslinked silica-casein aerogels (SC5 / SC5F and SC30 / SC30F in Fig. 1).

3.1.2. Infrared spectroscopy (FT–IR)

The FT-IR spectra of the hybrid silica-casein aerogels and that of the starting material casein MPI-85 are shown in Figs. 2 and S1 in the Supporting information. A broad band is present at 1000 cm^{-1} in all spectra, which is attributed to the Si–O–Si antisymmetric stretching vibration. The symmetric and the asymmetric vibrations of the carboxylate and amide groups are between 1646 and 1657 cm^{-1}. By comparing the intensity of the corresponding ν(C = O) peaks, it is clear that the amount of incorporated casein is much higher in the SC30 samples than in the SC5 samples. The FT-IR spectra of the cross-linked and the pristine aerogels are only slightly different. This can be explained by considering that only a few new crosslinking bonds form in the reaction of formaldehyde and casein, and the vibrations of these overlap with the much more intensive vibrations of the backbones. There is a noticeable decrease in relative intensity of the minor peak around 950 cm^{-1} of the SC30F sample compared to the SC30 sample, that can be attributed to the depletion of the Si–OH bonds due to their reaction with formaldehyde.

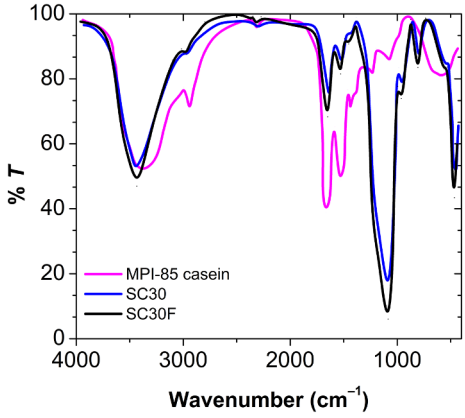

Fig. 2. Infrared spectra (FT-IR) of SC30 silica-casein aerogels and MPI-85 casein.

3.1.3. N_2 adsorption-desorption porosimetry

Representative N_2 adsorption-desorption isotherms of pristine and crosslinked silica-casein aerogels are shown in Figs. 3 and S2 in the Supporting Information. All hysteresis curves can be classified as IUPAC IV category with a H3 type loop, which is characteristic for mesoporous materials with a small number of macropores [66]. There is no steep rise in the isotherms at $p/p_0 = 1$, which indicates that the contribution of macropores to the measured porosity is negligible. According to the *t*-plot method, the contribution of micropores is also negligible to the total porosity [67]. All desorption curves return to zero relative pressure, meaning that the rigidity of the aerogel backbones is intact during the measurements and no deformation takes place that could falsify data evaluation. The structural parameters calculated from the isotherms by the BET and the BJH methods are given in Table 2. The specific surface areas (S_{BET}) of the aerogels are between 612 and 768 m^2/g. These values are relatively large considering that the parent silica aerogel has a specific surface area of 810 m^2/g [41]. The specific surface area of the hybrid aerogels decreases with the increase of their casein content. This can be the consequence of the formation of tightly packed sites in the structures of the SC30 and SC30F aerogels, as

Table 2
Structural parameters of silica-casein aerogels estimated by the BET and the BJH methods from N_2 adsorption-desorption porosimetry data (cf. Figs. 3 and S2).

Parameter	SC5	SC30	SC5F	SC30F	Data evaluation
C-constant	70.7	58.3	82.8	57.9	BET
Specific surface area (m^2/g)	750	612	768	616	BET
Average pore size (nm)	17.3	19.9	23.1	19.8	BJH
Total pore volume (cm^3/g)	3.22	3.03	4.47	3.05	BJH

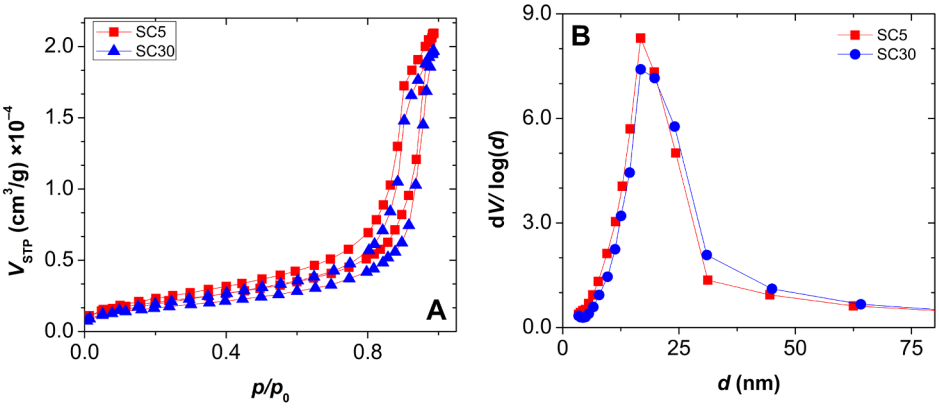

Fig. 3. Panel A: Nitrogen adsorption desorption isotherms of pristine silica-casein aerogels. Panel B: pores size distribution curves calculated from the desorption isotherms by using the BJH method. Additional data are given in Fig. S2 in the Supporting Information. Estimated structural parameters are summarized in Table 2.

pointed out in the SEM images (cf. Fig. 1). The S_{BET}, mean pore size and total pore volume values and of the crosslinked aerogels (SC5F and SC30F) are slightly higher, than those of the pristine hybrids. This indicates that the pore structure slightly opens up as the consequence of the formaldehyde treatment. This is also shown by the SANS results (vide infra in Section 3.1.4).

The BET *C*-constant is typically between 80 and 100 for silica aerogels. The silica-casein aerogels have smaller *C*-constants, and the value of this parameter decreases with increasing casein content (Table 2). Casein molecules have large nonpolar moieties, that can be responsible for the smaller values of the *C*-constant. The reaction with formaldehyde results in an increase in the *C*-constant, but only in the aerogel of low casein content (SC5). It is reasonable to assume that a higher portion of the protein can react and form crosslinks (new –C = O bonds) in the low-casein hybrid, which in turn results in an increase of surface polarity. Pore size distribution curves were calculated by the BJH method from the desorption isotherms (Fig. 3). These curves are practically equivalent for all hybrid aerogels with a mean pore size of ca. d_{pore} = 20 nm.

3.1.4. SANS of dry aerogels

Small angle neutron scattering (SANS) yields meaningful information on the structure of a heterogeneous sample if the characteristic inhomogeneities of the sample are nanometer sized and have different neutron scattering length densities [47,68]. The primary contrast in aerogels occurs between the solid backbone and the fluid phase inside the pores, i.e. air in the case of dry samples. In the case of a hybrid aerogel, the different components of the backbone can give a secondary contrast.

Small angle neutron scattering curves of dry silica-casein aerogels are shown in Fig. 4. All of the experimental curves can be adequately fitted with the Beaucage model (eq. (3)). The estimated values of the gyration radius (R_g) and the power law exponent (p) are given in Table 3. The values of the power law exponent are between 2 and 3 for the silica-casein aerogels of low casein content (SC5 and SC5F), which is characteristic for mass fractals [69,70]. The power law exponent is close to 3 for the hybrids of high casein content (SC30 and SC30F), which indicates that these aerogels can be approximated by surface fractals. A slight morphological difference was revealed by SEM between the hybrids of low and high casein contents, i.e. a small number of densely packed ridges are present in the 30 wt% casein hybrids (Fig. 1). This morphological difference is a feasible explanation for the alteration of the power law exponent by changing casein content. The value of the gyration radius is lower in the case of the aerogel of lower casein content (SC5F), but it does not change significantly as a consequence of formaldehyde treatment. In this sense, the R_g value inversely correlates with the S_{BET} value of the aerogels (cf. Section 3.1.3).

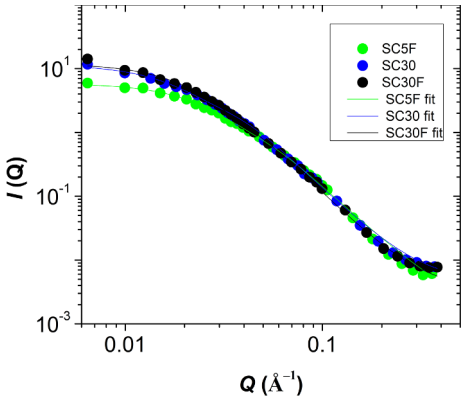

Fig. 4. Small angle neutron scattering (SANS) curves of silica-casein hybrid aerogels measured in their dry states. Solid lines represent data fitting with the Beaucage model. The estimated values of structural parameters are given in Table 3.

The SANS results strongly support the conclusions drawn from the SEM and the N_2 porosimetry data, i.e. the casein content and crosslinking have only minor effects on the nanostructures (i.e., the morphology and the pore size distribution) of the silica-casein aerogels.

The scattering curves of dry silica-casein aerogels do not show features distinct from silica aerogels, meaning that the backbones of the different hybrids scatter as homogeneous materials. The homogeneity of the aerogel backbones was studied further by contrast variation SANS experiments, which is detailed later in Section 3.4.2.

3.2. Compressive strength and flexibility of dry aerogels

Flexibility tests were performed at 2 different, arbitrary chosen points on each aerogel monolith. In general, the results of the duplicate tests are in good agreement with each other, regardless of the composition of the aerogel sample. This suggests, that the monoliths are crack free and homogeneous at the macroscopic level. Depth of deformation versus mass of load curves are given in Fig. 5. The depth of deformation at 50 g load was interpolated from the experimental curves (Table 4). These data suggest that the amount of casein in the backbone has practically no effect on the flexibility of the aerogel monoliths, but crosslinking by formaldehyde results in an increase of rigidity.

Representative strain–stress curves of silica-casein aerogels are shown in Fig. 5, and the corresponding compressive strength values are given in Table 4. Strain is practically proportional to stress in the case of the aerogels of low casein content, while the curves of the high casein aerogels show breaks at several points, which indicates the extensive formation of micro-cracks. Crosslinking by formaldehyde significantly

Table 3
The values of the gyration radius (R_g) and the power law exponent (p) for dry and hydrated silica-casein aerogel samples. Parameters were estimated by fitting experimental small angle neutron scattering (SANS) curves with the Beaucage model (eq. (3)).

	dry	hydrated(H_2O)	hydrated(2:1 H_2O:D_2O)
SC5F	R_g = 67 ± 2 Å p = 2.6 ± 0.1	R_g = 77 ± 3 Å p = 2.8 ± 0.1	R_g = 59 ± 2Å p = 3.0 ± 0.1
SC30	R_g = 78 ± 2 Å p = 3.1 ± 0.1	R_g = 93 ± 3 Å p = 2.5 ± 0.1	R_g = 68 ± 2Å p = 2.6 ± 0.1
SC30F	R_g = 81 ± 2 Å p = 3.0 ± 0.1	R_g = 98 ± 3 Å p = 2.6 ± 0.1	R_g = 70 ± 2Å p = 2.6 ± 0.1

increases the compressive strength of the hybrid aerogel of low casein content, but has practically no effect in the case of the high casein aerogel.

The compiled results of the mechanical tests suggest that the silica-casein aerogels increase both in compressive strength and rigidity at high casein content, and both of these properties display a further, minor increase upon crosslinking by formaldehyde. The monolith of the crosslinked silica-casein aerogel of low casein content (SC5F) displays optimal mechanical properties. The compressive strengths of the hybrids are higher than those of the archetypical silica aerogels [71–73].

Table 4
Results of the duplicate flexibility tests and compressive strength tests.

Code	Depth of deformation at 50 g load (mm) 1st test	2nd test	Compressive strength (kPa)
SC5	1.34	1.10	52
SC30	1.24	1.62	32
SC5F	0.87	0.93	74
SC30F	0.93	0.96	23
silica			34

3.3. Particle size and Zeta potential of hydrated aerogels

Silica-casein aerogels spontaneously disintegrate in water and yield micrometer-sized particles. In order to increase the reproducibility of the disintegration of the aerogels, wet grinding was applied to produce suspensions. The size distribution curves of the suspended particles are practically equivalent for all hybrid aerogels with mean particle sizes between 12 and 18 μm, regardless of their casein content and the presence of crosslinking (Fig. S3 in the Supporting Information).

The Zeta potential (E_Z) of the hybrid aerogel particles was measured in the pH range from 3.0 to 9.0. Data are summarized in Fig. S4 in the Supporting Information. In general, the Zeta potential of the hybrid aerogels is negative above pH 3.5. (This pH value is the approximate isoelectric point of silica [74]). The approximate isoelectric point of casein is pH 4.5 [75]. The E_Z values of all hybrid aerogels are ca. −30 mV at pH = 7.0 and only slightly change with changing chemical composition. The pristine aerogel of low casein content (SC5) has the lowest E_Z values among the hybrids, regardless of pH. Crosslinking by formaldehyde slightly increases E_Z at each pH value.

3.4. Structural characteristics of hydrated aerogels

3.4.1. Morphology of hydrated aerogels by SANS

Silica-casein aerogels were hydrated by adding 3.5 g H_2O to 1.0 g aerogel. This amount of water fully hydrates the backbone and saturates the pores, as shown by the NMR cryoporometry measurements (cf. Section 3.4.3). The corresponding SANS scattering curves are almost identical with those measured in the dry states of the aerogels (cf. Fig. 4) The structural parameters (R_g and p) estimated with the Beaucage model are given in Table 3. The value of the power law exponent (p) does not change significantly by the hydration of the aerogels, while the value of the gyration radius increases for all hybrids. However, the increase of the value of R_g is negligible compared to the hydration induced alteration of the R_g values of such silica-gelatin aerogels that significantly swell on the microscopic level upon hydration [41]. In the case of the silica-casein aerogels, the minor increase of the R_g value is attributed to the formation of the hydration sphere of the solid backbone, that is well expressed in the NMR relaxometry data, as well (cf. Section 3.4.4). Practically, there is no difference between the nature of the hydration induced minor structural changes in the pristine and the crosslinked hybrid aerogels. Thus, the high similarity of the scattering curves of the dry and the hydrated silica-casein aerogels indicates that the porous structures of the hybrids are practically not altered upon hydration. There are no signs of the collapse or the swelling of the aerogel networks [76,77].

3.4.2. Homogeneity of aerogel backbone by SANS

Independent contrast variation experiments were performed by hydrating the silica-casein aerogels with H_2O:D_2O 2:1 (64 wt% H_2O and 36 wt% D_2O) mixture (3.5 g liquid / g aerogel). The neutron scattering length density (SLD) values of silica, bovine casein and H_2O:D_2O 2:1 mixture are estimated to be 4.10 × 10^{-6} $Å^{-2}$, 1.96 × 10^{-6} $Å^{-2}$ and 1.90 × 10^{-6} $Å^{-2}$, in order [78,79]. It has been reported that the scattering of casein micelles is matched by a mixture of 60 wt% H_2O and 40 wt% D_2O [78]. Thus, it is valid to assume that the neutron scattering length density of the casein component of the hybrid aerogel is

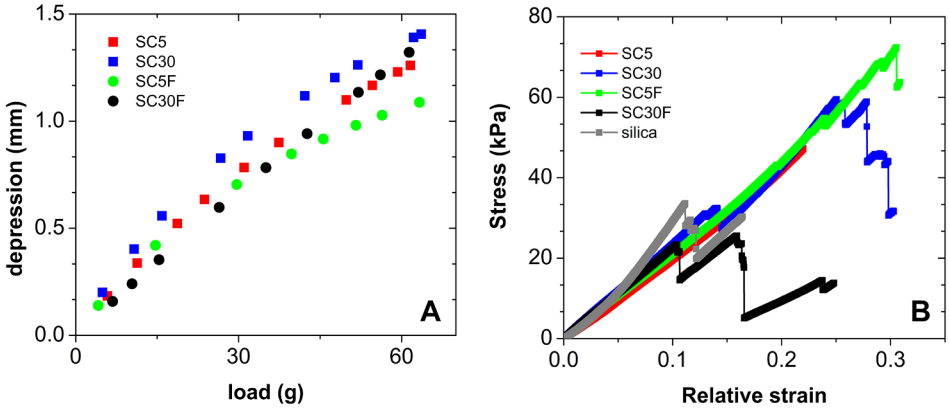

Fig. 5. Flexibility tests (panel A) and compressive strength tests (panel B) of pristine and crosslinked silica-casein hybrid aerogel monoliths.

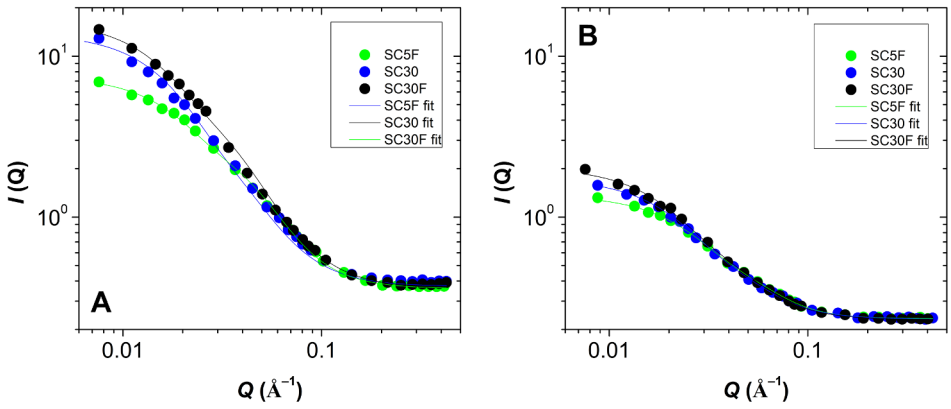

Fig. 6. Small angle neutron scattering (SANS) curves of fully hydrated silica-casein aerogels. Panel A: Silica-casein aerogels hydrated by H_2O (3.5 g liquid / g aerogel). Panel B: Silica-casein aerogels hydrated by H_2O:D_2O 2:1 mixture (3.5 g liquid / g aerogel). Solid lines represent data fitting with the Beaucage model. The estimated structural parameters are given in Table 3.

approximately the same as that of the liquid H_2O:D_2O 2:1 mixture. Indeed, the scattering intensity of the wet silica-casein aerogel hydrated by H_2O:D_2O 2:1 is one order of magnitude lower, then that of the wet silica-casein aerogel hydrated by pure H_2O (Fig. 6).

Nevertheless, the scattering curves are still structured, and can be fitted with the Beaucage model. The values of the power law exponent (p) are similar to those that are characteristic for the silica-casein aerogels in the dry sate, while the R_g values are lower than in the dry state (Table 3). This indicates, that the main structural features and the spatial distribution of the silica component in the hybrid backbone is practically the same as in the dry state of the material. Still, the SANS contrast of silica remains distinct in the wet hybrid backbones when hydrated by H_2O:D_2O 2:1 mixture. When the contrast is reduced, the scattering pattern does not change significantly, that suggests that silica and casein do not form separate nanometer domains of different shapes and mix on the nanometer scale. This is a strong indication that the hybridizations of the different silica-casein backbones are homogeneous on the nanometer scale. Thus, the silica-casein hybrids can be regarded as homogeneous nanocomposites where the individual silica and casein building blocks are smaller than the spatial resolution of the SANS and the SEM techniques.

It is interesting to note, that the R_g values are somewhat higher when the hybrid aerogels are hydrated by H_2O and lower when they are hydrated by H_2O:D_2O 2:1 mixture compared to the dry states of the materials (Table 3). One explanation could be that some of the smaller pores are not filled with water upon the hydration of the aerogel matrix, but this explanation is in contradiction with the NMR relaxometry results. (NMR relaxometry data strongly suggest that the filling of the pores is continuous and there are no preferences in the wetting of the smaller and larger pores, as discussed in Section 3.4.4.) A more feasible explanation is that a thick water layer forms in association with the hybrid backbone as the primary hydration sphere that yields nanometer scale density differences near the surface of the solid backbone, and this phenomenon is highlighted by the variation of the contrast.

3.4.3. NMR cryoporometry

The pore size distributions of hydrated silica-casein aerogels were determined by NMR cryoporometry at water contents of 5.0 g H_2O / 1.0 g dry aerogel. A representative melting-freezing curve is shown in Fig. 7A for SC5. The ratio of the height of the two steps in the cryoporometry curve indicates that the ratio of pore water and bulk water is ca. 1:1.7 in the sample of 5.0 g/g water content. Water in the pores melts at 267.9 K and freezes at 264.9 K. The difference between the melting and the freezing points of pore water and the melting point of bulk water is 5.2 and 8.2 K, respectively. These differences represent a 2:3 ratio, which indicates the dominating presence of spherical pores in the hydrated aerogel [54–56,80]. Similar hysteresis curves were obtained for each hybrid aerogel. Pore size distribution curves were calculated by using K_c = 30 nm K for water in the Gibbs-Thompson equations (eq. (4)) [81–83]. The mean diameter of the pores is around 20 nm for each hydrated silica-casein aerogel as seen in Fig. 7B.

Thus, the pore size distribution curves of the hydrated aerogels are in good agreement with those measured by N_2 porosimetry in the dry states of the aerogels. In the case of the SC30F aerogel, slightly smaller pore sizes were measured in the hydrated state of the aerogel than by N_2 porosimetry. This indicates the slight loss of hydrophilicity of the crosslinked SC30F silica-casein compared to the pristine hybrid. Overall, NMR cryoporometry data show that the porous structures of the silica-casein hybrid aerogels remain intact even when the matrices are fully hydrated and the pores are completely filled by water [65,84,85]. This conclusion is in complete agreement with the those drawn from the results of the SANS measurements (Section 3.4.1).

3.4.4. NMR relaxometry

The T_2 (spin–spin) relaxation time of water significantly depends on the extent of interactions of water molecules with solid surfaces. Accordingly, when a porous solid matrix is gradually hydrated (i.e. its water content is increased until the saturation of the pores), the accompanying change of the T_2 relaxation time of water conveys information on the wetting mechanism of the solid backbone and on the porous structure of the system [49,51,53].

Silica-casein aerogels were gradually hydrated, and the T_2 relaxation time of water was recorded as function of water content. The saturation of the pores is reached at water content of 3.4 g water / 1.0 g dry aerogel. In general, the NMR relaxometry data is almost identical for all silica-casein aerogels, regardless of their chemical composition. Two well-separated relaxation domains can be detected in all hydrated aerogels even at the lowest water content, as seen in Fig. 8. The domain with the smaller T_2 is attributed to solvent molecules in strong interaction with the surface of the aerogels, i.e. the primary hydration sphere of the silica-casein backbone [86,87]. Accordingly, the value of the smaller T_2 relaxation time is practically independent of the water content of the aerogel. [88] The higher T_2 values are attributed to the average relaxation of water molecules moving relatively freely inside the pores. The higher T_2 increases monotonously with increasing water content, because the constraint of the molecules decreases due to the formation of quasi bulk phases by filling the pores. [49–53,89] It is interesting to note, that the amplitudes of the 2 relaxation domains are in close correlation with each other (Fig. 8B). The most feasible explanation for this phenomenon is that water molecules exchange between the 2 domains by an intermediate-slow rate. [87] Otherwise, in the case of limiting slow exchange, the amplitude of the high T_2 domain would monotonously increase with increasing water content. In the case of limiting fast exchange, the 2 domains would not be separable and merge into a single average domain. [49,51,53]

The above described hydration mechanism is effective in the case of all silica-casein aerogels, and it is typical for hydrophilic mesoporous silica materials. [90,91] The first step is the formation of a thin, but

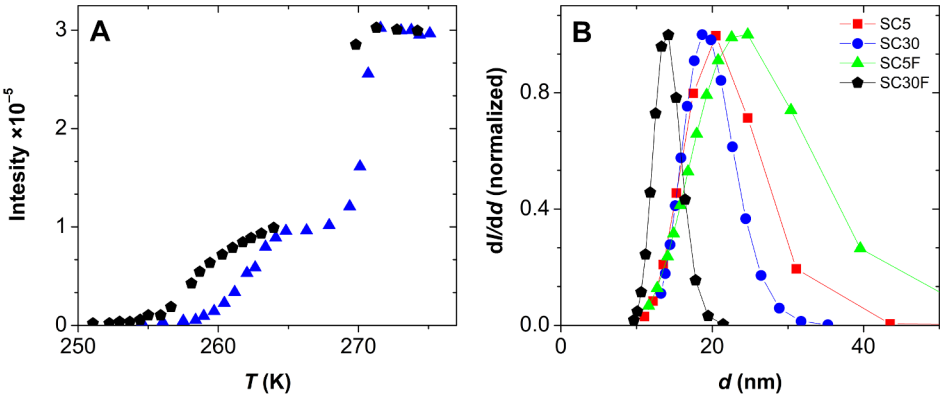

Fig. 7. NMR cryoporometry of hydrated silica-casein aerogels. Panel A: Intensity of the water signal as function of temperature during the melting (blue) and the freezing (black) processes of the hydrated SC5 aerogel. Panel B: Pore size distribution curves calculated from the intensity data using the modified Gibbs-Thompson equations (eq. (4)).

well-defined water layer at the surface of the aerogel backbone. The saturation of this primary hydration sphere (at ca. 0.2 g/g water content) is followed by puddle formation in focal points inside the pores. [49] When water content increases, the puddles are connected into a coherent fluid layer inside the pores, and partially fill these. The reciprocal filling-factor plots (Fig. S5 in the Supporting Information) suggest that the subsequent saturation of the pores by water is a gradual, monotonous process in each aerogel. [51]

By compiling the results of NMR relaxometry, two main conclusions can be drawn. 1) The hydration mechanism of all hybrid silica-casein aerogels is practically the same as that of archetypical mesoporous silica materials. 2) Neither the amount of the incorporated casein, nor the application of crosslinking agents have a detectable effect on this hydration mechanism.

3.4.5. NMR diffusiometry

The self-diffusion of water in hydrated aerogels can be measured by PGSE NMR technique. In general, the apparent self-diffusion coefficient (D_{obs}) of a liquid filling the pores of a solid matrix differs from the D_{obs} value effective in the bulk phase of the liquid due to the confinement of the molecules by the pore walls. The presence of multiple diffusion domains indicates that the permeability of the hydrated porous solid is low, hence the confinement of water is not uniform in the sample. On the other hand, a single average D_{obs} is characteristic for highly permeable porous solids, where the exchange of water molecules is fast among the different structural regions of the sample. [62,64,92] The apparent self-diffusion coefficient of water also depends on the length of the observation time of the diffusion experiment, because on a longer timescale the molecules bounce back from the walls repeatedly, which decreases their effective displacement. [59,63,64]

Silica-casein aerogels were studied at 3 different hydration levels: 0.5, 1.3 and 3.2 g water / 1.0 g dry aerogel. Furthermore, the observation time of the diffusion measurement was varied between 10 and 140 ms for all samples. Independently of the observation time, and also independently of the water content of the hydrated aerogels, only one diffusion domain was detected in all samples (Fig. 9A). However, this single D_{obs} value increases with the increasing water content of the hydrated aerogels, regardless of their chemical composition. This behavior is possible only, if water molecules of different spatial localization are in fast exchange with each other on the timescale of diffusiometry. [93] These results strongly suggest that the porous structure of the hydrated silica-casein aerogels are open and highly permeable, as it is in the case of the hydrated parent silica aerogel. [65,94]

The values of D_{obs} measured at different levels of hydration systematically correlate with the chemical compositions of the silica-casein aerogels (Fig. 9B). That is, the D_{obs} values are lower at high casein content, and lower when crosslinking is applied, indicating the lower permeability of these hydrated matrices. [95] As the pore size distributions and the hydration mechanisms are practically the same for all variants of hydrated silica-casein aerogels, the decrease in D_{obs} is attributed to a higher tortuosity of the high casein content and the crosslinked aerogels. For comparison, the D_{obs} value measured in the fully hydrated parent silica aerogel is 1.9×10^{-5} cm^2 s^{-1}, while that is 1.8×10^{-5} cm^2 s^{-1} in the fully hydrated SC5 hybrid and 2.3×10^{-5} cm^2 s^{-1} in bulk water. [65,96]

3.4.6. Unique behavior of silica-casein aerogels in water

As a summary of the aqueous phase characterization of silica-casein aerogels, it can be stated that the structural properties of these hydrated hybrids are almost identical to those of the hydrated parent silica aerogel. [49,65] This is a unique feature for hybrid inorganic-biopolymer materials.

The hydrated silica-casein aerogel particles retain their open mesoporous structures, even when completely hydrated and filled with

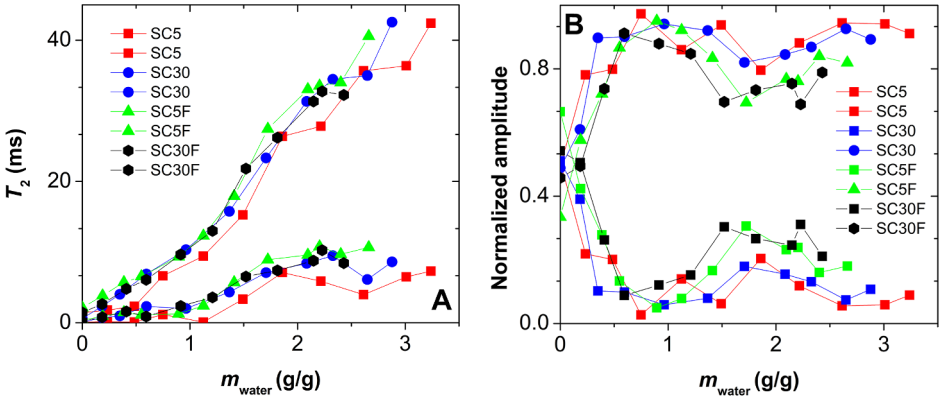

Fig. 8. NMR relaxometry of hydrated silica-casein aerogels. Panel A: Experimental T_2 relaxation times of water as function of water content of hydrated aerogels. Panel B: The normalized amplitudes corresponding to the relaxation processes shown in panel A.

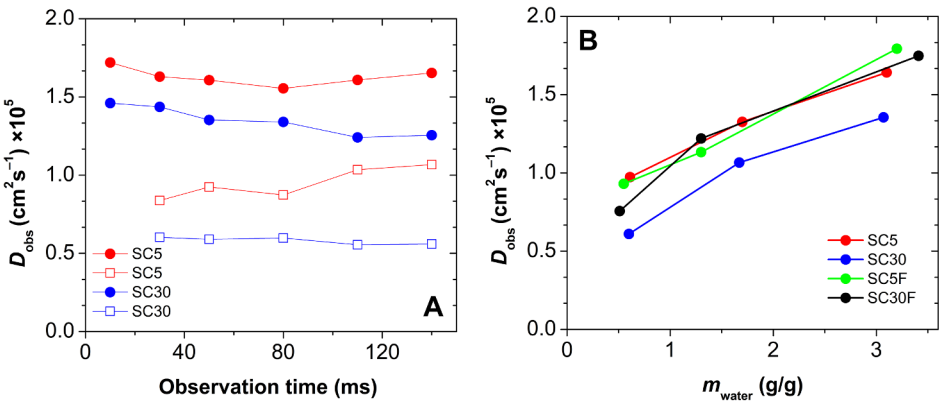

Fig. 9. Self-diffusion of water in hydrated silica-casein aerogels measured by NMR diffusiometry. Panel A: Observation time dependence of the self-diffusion coefficient (D_{obs}) of hydrated SC5 (red) and SC30 (blue) aerogels at two different water contents (open symbol: 0.6 g/g; filled symbol: 3.1 g/g). Panel B: Dependence of D_{obs} on the water contents of the hybrid aerogels.

water. This behavior is almost independent of the casein content of the aerogel or its state of crosslinking. Even partial hydration induces the immediate disintegration of the silica-casein aerogel monoliths into microparticles ($d_{particle}$ = 15 μm in average). The pores of the hydrated particles are highly permeable for water, and the morphologies and pore size distributions of the hydrated aerogels are the same as in their dry states. This is highly unusual for inorganic-biopolymer hybrids. [26,41] The hydration of the protein components usually causes the extensive swelling and deformation of the solid backbone of the hybrid, that results in the partial or complete collapse of the pore structure. [89,97–99]

3.5. Biocompatibility of silica-casein aerogels

Biocompatibility tests of pristine silica-casein aerogels (SC5 and SC30) were performed on CHO-K1 cell cultures. The SC5F and the SC30F aerogels were excluded, because even traces of leftover formaldehyde would compromise the study. The cell cultures were monitored by a time-lapse imaging near-infrared microscopy system. Cell viability was quantified by the MTT assay. Pre-conditioned silica-casein aerogel particles and 1 – 2 mm thick aerogel slabs were used. [100]

The time-lapse imaging experiments were conducted for 40 h. In addition to monitoring the growth of the CHO-K1 cell cultures, 10 – 10 individual cells were tracked in the control and in the silica-casein aerogel containing sequences of the time-lapse scans. In general, both the control and treated cell cultures reached nearly 100% confluency. The lag phase was longer in the case of treated cells, but the cells finally covered the available space in the cell culture flask (Fig. S6 in the Supporting Information). No detectable difference can be seen in the dividing time and in the generation time between the control and treated cells (Fig. S7 in the Supporting Information). The mean migration pathways of the cells in the vicinity of aerogel particles were the same as in the control culture (control: 160 ± 32, SC30: 145 ± 28, SC5: 162 ± 21). The migration plots did not show significant difference in the direction of the migration of the cells in the presence of the aerogel particles (Fig. S8 in the Supporting Information). The time-lapse imaging scans showed no signs of apoptosis or necrosis at different phases of the cell cycle in the presence of the silica-casein aerogel particles (Fig. 10).

The MTT assay results showed that none of the studied silica-casein aerogel microparticles caused a significant decrease in the viability of the CHO-K1 cells. A slight decrease of cell viability was observed at an aerogel concentration of 0.5 mg/mL, which decreased further at 1.0 mg/mL aerogel concentration (Fig. 11). This is probably due to the physical stress caused by the high concentration of the aerogel particles, that disturbed the normal adherence of the cells.

Based on the time-lapse imaging and the MTT assay results, the silica-casein aerogel particles are highly biocompatible with the CHO-K1 cells and practically inert in the biological context. Previous biocompatibility experiments were performed with silica-gelatin hybrid aerogels. The gelatin containing hybrids show chemoattractant properties towards adhesive cell types, and the adhesion of these cells is facile on the surface of the gelatin containing aerogels. [25,27] A feasible explanation for the differences between the properties of the two families of hybrid aerogels can be that the surface charge (i.e. the Zeta potential) of the silica-casein particles are much more negative that of the silica-gelatin particles: ca. −30 mV and ca. −20 mV, respectively. Also, gelatin and collagen are well-known chemoattractants, while bovine casein is practically inert in this sense.

4. Conclusions

Silica-casein hybrid aerogels can be conveniently synthesized by a sol-gel method when the hydrolysis and polycondensation of the silica precursor (TMOS) takes place in the presence of dissolved casein. The chemical crosslinking of the hybrid backbone can be achieved by adding formaldehyde to the alcogels during solvent exchange. Supercritical drying in CO_2 yields crack-free hybrid aerogel monoliths with casein contents up to 28 wt%.

Nitrogen adsorption-desorption porosimetry, SEM and SANS measurements revealed that the microscopic morphologies of the hybrid silica-casein aerogels are almost identical to that of the parent silica aerogel. Primary globules of $d_{globule}$ = 15 – 20 nm are connected into an open network of mesopores. The characteristic specific surface of the aerogels is ca. 700 m^2/g, and the mean pore diameter is ca. 20 nm. These structural parameters slightly decrease with the increasing casein content of the aerogels, but the main morphological features are practically independent of casein content and the state of crosslinking. Contrast variation SANS experiments revealed that silica and casein are hybridized on the nanometer scale and form homogeneous nanocomposites.

The rigidity and the compressive strength of the silica-casein aerogels are similar to that of the parent silica aerogel. The crosslinked hybrid aerogel of 5 wt% casein content has the best mechanical properties.

All hybrid aerogels disintegrate in a similar manner in water to form hydrated microparticles (d = 15 μm in average) of large negative Zeta potentials (-30 mV in average at pH = 7.0). The combination of SANS, and NMR cryoporometry, relaxometry and diffusiometry measurements revealed that silica-casein aerogels retain their open, permeable mesoporous structures in water, even when completely hydrated, regardless of casein content or the state of crosslinking. The morphologies and the pore size distributions of the hydrated aerogel particles are the same as in their dry state. This is unusual for inorganic-biopolimer hybrids. The hydration of protein components often causes the extensive swelling and deformation of the solid backbone, that results in the partial or complete collapse of the pore structure. Thus, silica-casein aerogels are unique regarding their characteristics in the hydrated state.

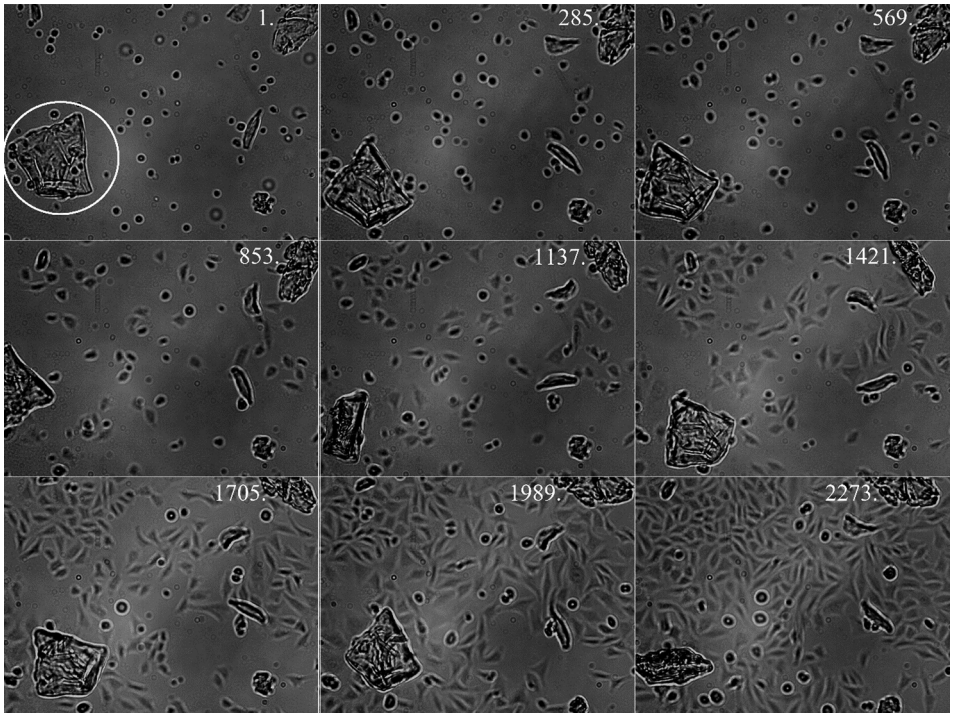

Fig. 10. Time-lapse near infrared microscopy imaging of a CHO-K1 cell culture in the presence of SC30 silica-casein aerogel particles (c_{agel} = 1.0 mg/mL). The white circle shows a silica-casein particle and the numbers on the corner of the images indicate the elapsed time in minutes.

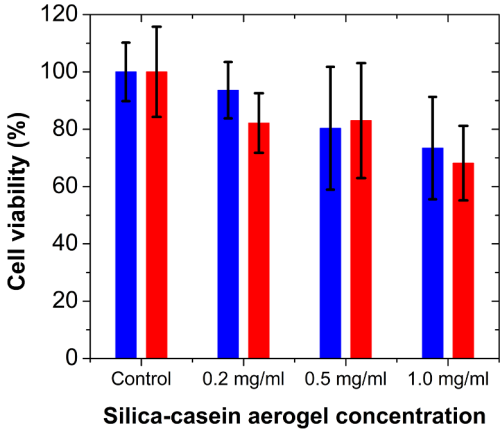

Fig. 11. Cell viability of CHO-K1 cell cultures in the presence of SC5 (red) and SC30 (blue) silica-casein aerogel particles measured by MTT assay. (The applied c_{agel} is given on the *x*-axis.)

Silica-casein aerogels are highly biocompatible and practically inert towards CHO-K1 cells. The hybrid particles do not act as chemoattractants against these cells.

As a final conclusion, the newly synthesized silica-casein hybrid aerogels display all the advantageous chemical and physical properties of pristine silica aerogels, and the protein component opens new possibilities for functionalization to better suite biomedical and engineering applications.

CRediT authorship contribution statement

István Lázár: Conceptualization, Data curation, Formal analysis. **Attila Forgács:** Data curation, Formal analysis, Visualization, Writing - original draft. **Anita Horváth:** Data curation, Formal analysis, Writing - original draft. **Gábor Király:** Data curation, Formal analysis. **Gábor Nagy:** Data curation, Formal analysis. **Adél Len:** Data curation, Formal analysis. **Zoltán Dudás:** Data curation, Formal analysis. **Vanda Papp:** Data curation, Formal analysis. **Zoltán Balogh:** Data curation, Formal analysis. **Krisztián Moldován:** Data curation, Formal analysis. **Laura Juhász:** Data curation, Formal analysis. **Csaba Cserháti:** Data curation, Formal analysis. **Zsuzsanna Szántó:** Conceptualization, Supervision, Resources, Project administration. **István Fábián:** Funding acquisition, Supervision, Resources, Project administration. **József Kalmár:** Conceptualization, Data curation, Formal analysis, Supervision, Validation, Visualization, Writing - original draft, Writing - review & editing.

Declaration of Competing Interest

The authors declare that they have no known competing financial interests or personal relationships that could have appeared to influence the work reported in this paper.

Acknowledgements

This research has been financially supported by the National Research, Development and Innovation Office, Hungarian Science Foundation (OTKA: FK_17-124571). J. Kalmár is grateful for the János Bolyai Research Scholarship of the Hungarian Academy of Sciences and for the New National Excellence Program (ÚNKP-19-4 Bolyai +) of the Ministry of Innovation and Technology of Hungary for financial support. The research was supported by the EU and co-financed by the European Regional Development Fund under the projects GINOP-2.2.1-15-2017-00068 and GINOP-2.3.2-15-2016-00041.

Appendix A. Supplementary data

Supplementary data to this article can be found online at https://doi.org/10.1016/j.apsusc.2020.147232.

References

[1] C.A. García-González, T. Budtova, L. Durães, C. Erkey, P. Del Gaudio, P. Gurikov, M.

Koebel, F. Liebner, M. Neagu, I. Smirnova, An Opinion Paper on Aerogels for Biomedical and Environmental Applications, Molecules, 24 (2019) 1815.
[2] C.A. García-González, C. López-Iglesias, A. Concheiro, C. Alvarez-Lorenzo, Biomedical Applications of Polysaccharide and Protein Based Aerogels, in: Biobased Aerogels, 2018, pp. 295-323.
[3] H. Maleki, L. Duraes, C.A. Garcia-Gonzalez, P. Del Gaudio, A. Portugal, M. Mahmoudi, Synthesis and biomedical applications of aerogels: Possibilities and challenges, Adv. Colloid Interface Sci. 236 (2016) 1–27.
[4] I. Smirnova, P. Gurikov, Aerogel production: Current status, research directions, and future opportunities, J. Supercrit. Fluid. 134 (2018) 228–233.
[5] J. Stergar, U. Maver, Review of aerogel-based materials in biomedical applications, J. Sol-Gel Sci. Technol. 77 (2016) 738–752.
[6] Z. Ulker, C. Erkey, An emerging platform for drug delivery: aerogel based systems, J. Control. Release 177 (2014) 51–63.
[7] H. Maleki, Recent advances in aerogels for environmental remediation applications: A review, Chem. Eng. J. 300 (2016) 98–118.
[8] G. Vasvari, J. Kalmar, P. Veres, M. Vecsernyes, I. Bacskay, P. Feher, Z. Ujhelyi, A. Haimhoffer, A. Rusznyak, F. Fenyvesi, J. Varadi, Matrix systems for oral drug delivery: Formulations and drug release, Drug. Discov. Today Technol., 27 (2018) 71-80.
[9] T. Budtova, Cellulose II aerogels: a review, Cellulose 26 (2019) 81–121.
[10] K. Ganesan, T. Budtova, L. Ratke, P. Gurikov, V. Baudron, I. Preibisch, P. Niemeyer, I. Smirnova, B. Milow, Review on the Production of Polysaccharide Aerogel Particles, Materials, 11 (2018) 2144.
[11] L. Goimil, M.E.M. Braga, A.M.A. Dias, J.L. Gomez-Amoza, A. Concheiro, C. Alvarez-Lorenzo, H.C. de Sousa, C.A. García-González, Supercritical processing of starch aerogels and aerogel-loaded poly (ε-caprolactone) scaffolds for sustained release of ketoprofen for bone regeneration, J. CO2 Util. 18 (2017) 237–249.
[12] V.S.S. Goncalves, P. Gurikov, J. Poejo, A.A. Matias, S. Heinrich, C.M.M. Duarte, I. Smirnova, Alginate-based hybrid aerogel microparticles for mucosal drug delivery, Eur. J. Pharm. Biopharm. 107 (2016) 160–170.
[13] S. Groult, T. Budtova, Tuning structure and properties of pectin aerogels, Eur. Polym. J. 108 (2018) 250–261.
[14] C. Lopez-Iglesias, J. Barros, I. Ardao, F.J. Monteiro, C. Alvarez-Lorenzo, J.L. Gomez-Amoza, C.A. Garcia-Gonzalez, Vancomycin-loaded chitosan aerogel particles for chronic wound applications, Carbohydr. Polym. 204 (2019) 223–231.
[15] S. Zhao, W.J. Malfait, N. Guerrero-Alburquerque, M.M. Koebel, G. Nystrom, Biopolymer Aerogels and Foams: Chemistry, Properties, and Applications, Angew. Chem. Int. Ed. 57 (2018) 7580–7608.
[16] P. Veres, D. Sebok, I. Dekany, P. Gurikov, I. Smirnova, I. Fabian, J. Kalmar, A redox strategy to tailor the release properties of Fe(III)-alginate aerogels for oral drug delivery, Carbohydr. Polym. 188 (2018) 159–167.
[17] C. Lopez-Iglesias, A.M. Casielles, A. Altay, R. Bettini, C. Alvarez-Lorenzo, C.A. Garcia-Gonzalez, From the printer to the lungs: Inkjet-printed aerogel particles for pulmonary delivery, Chem. Eng. J. 357 (2019) 559–566.
[18] T. Athamneh, A. Amin, E. Benke, R. Ambrus, C.S. Leopold, P. Gurikov, I. Smirnova, Alginate and hybrid alginate-hyaluronic acid aerogel microspheres as potential carrier for pulmonary drug delivery, J. Supercrit. Fluid. 150 (2019) 49–55.
[19] H. Maleki, N. Huesing, Silica-silk fibroin hybrid (bio) aerogels: two-step versus one-step hybridization, J. Sol-Gel Sci. Technol. 1–9 (2019).
[20] H. Maleki, M.A. Shahbazi, S. Montes, S.H. Hosseini, M.R. Eskandari, S. Zaunschirm, T. Verwanger, S. Mathur, B. Milow, B. Krammer, N. Husing, Mechanically Strong Silica-Silk Fibroin Bioaerogel: A Hybrid Scaffold with Ordered Honeycomb Micromorphology and Multiscale Porosity for Bone Regeneration, ACS Appl. Mater. Interfaces, 11 (2019) 17256-17269.
[21] Z. Ulker, C. Erkey, A novel hybrid material: an inorganic silica aerogel core encapsulated with a tunable organic alginate aerogel layer, RSC Adv. 4 (2014) 62362–62366.
[22] H.B. Chen, B.S. Chiou, Y.Z. Wang, D.A. Schiraldi, Biodegradable pectin/clay aerogels, ACS Appl. Mater. Interfaces 5 (2013) 1715–1721.
[23] W. Li-Hong, C. Xin, X. Hui, Z. Li-Li, H. Jing, Z. Mei-Juan, L. Jie, L. Yi, L. Jin-Wen, Z. Wei, C. Gang, A novel strategy to design sustained-release poorly water-soluble drug mesoporous silica microparticles based on supercritical fluid technique, Int. J. Pharm. 454 (2013) 135–142.
[24] M. Pantic, Z. Knez, Z. Novak, Supercritical impregnation as a feasible technique for entrapment of fat-soluble vitamins into alginate aerogels, J. Non-Cryst. Solids 432 (2016) 519–526.
[25] G. Nagy, G. Kiraly, P. Veres, I. Lazar, I. Fabian, G. Banfalvi, I. Juhasz, J. Kalmar, Controlled release of methotrexate from functionalized silica-gelatin aerogel microparticles applied against tumor cell growth, Int. J. Pharm. 558 (2019) 396–403.
[26] P. Veres, M. Keri, I. Banyai, I. Lazar, I. Fabian, C. Domingo, J. Kalmar, Mechanism of drug release from silica-gelatin aerogel-Relationship between matrix structure and release kinetics, Colloid. Surface. B 152 (2017) 229–237.
[27] P. Veres, G. Kiraly, G. Nagy, I. Lazar, I. Fabian, J. Kalmar, Biocompatible silica-gelatin hybrid aerogels covalently labeled with fluorescein, J. Non-Cryst. Solids 473 (2017) 17–25.
[28] P. Veres, A.M. Lopez-Periago, I. Lazar, J. Saurina, C. Domingo, Hybrid aerogel preparations as drug delivery matrices for low water-solubility drugs, Int. J. Pharm. 496 (2015) 360–370.
[29] P. Herman, I. Fábián, J. Kalmár, Mesoporous Silica-Gelatin Aerogels for the Selective Adsorption of Aqueous Hg(II), ACS Appl. Nano Mater. (2020).
[30] A. Carr, M. Golding, Functional Milk Proteins Production and Utilization: Casein-Based Ingredients, in: P.L.H. McSweeney, J.A. O'Mahony (Eds.), Advanced Dairy Chemistry: Volume 1B: Proteins: Applied Aspects, Springer, New York, New York, NY, 2016, pp. 35–66.
[31] A. Ghosh, M.A. Ali, G.J. Dias, Effect of cross-linking on microstructure and physical performance of casein protein, Biomacromolecules 10 (2009) 1681–1688.
[32] T. Pojanavaraphan, R. Magaraphan, B.S. Chiou, D.A. Schiraldi, Development of biodegradable foamlike materials based on casein and sodium montmorillonite clay, Biomacromolecules 11 (2010) 2640–2646.
[33] D.A. Schiraldi, Green Polymer Aerogels, in: Green Polymer Chemistry: Biobased Materials and Biocatalysis, American Chemical Society, 2015, pp. 471-482.
[34] M. Chen, G. Sala, H.J.F. van Valenberg, A.C.M. van Hooijdonk, E. van der Linden, M.B.J. Meinders, Foam and thin films of hydrophilic silica particles modified by beta-casein, J. Colloid Interface Sci. 513 (2018) 357–366.
[35] A. Gurikov, A. Kolnoochenko, M. Golubchikov, N. Menshutina, I. Smirnova, A synchronous cellular automaton model of mass transport in porous media, Comput. Chem. Eng. 84 (2016) 446–457.
[36] R. Mellaerts, E.J. Fayad, G. Van den Mooter, P. Augustijns, M. Rivallan, F. Thibault-Starzyk, J.A. Martens, In situ FT-IR investigation of etravirine speciation in pores of SBA-15 ordered mesoporous silica material upon contact with water, Mol. Pharm. 10 (2013) 567–573.
[37] T. Ukmar, U. Maver, O. Planinsek, V. Kaucic, M. Gaberscek, A. Godec, Understanding controlled drug release from mesoporous silicates: theory and experiment, J. Control. Release 155 (2011) 409–417.
[38] G. Vigil, Z. Xu, S. Steinberg, J. Israelachvili, Interactions of Silica Surfaces, J. Colloid Interface Sci. 165 (1994) 367–385.
[39] A. Tzur-Balter, J.M. Young, L.M. Bonanno-Young, E. Segal, Mathematical modeling of drug release from nanostructured porous Si: combining carrier erosion and hindered drug diffusion for predicting release kinetics, Acta Biomater. 9 (2013) 8346–8353.
[40] V. Uskokovic, Mechanism of formation governs the mechanism of release of antibiotics from calcium phosphate nanopowders and cements in a drug-dependent manner, J. Mater. Chem. B 7 (2019) 3982–3992.
[41] M. Keri, A. Forgacs, V. Papp, I. Banyai, P. Veres, A. Len, Z. Dudas, I. Fabian, J. Kalmar, Gelatin content governs hydration induced structural changes in silica-gelatin hybrid aerogels - Implications in drug delivery, Acta Biomater. (2020).
[42] T. Benselfelt, L. Wagberg, Unidirectional Swelling of Dynamic Cellulose Nanofibril Networks: A Platform for Tunable Hydrogels and Aerogels with 3D Shapeability, Biomacromolecules 20 (2019) 2406–2412.
[43] Y. Kharbanda, M. Urbanczyk, O. Laitinen, K. Kling, S. Pallaspuro, S. Komulainen, H. Liimatainen, V.V. Telkki, Comprehensive NMR Analysis of Pore Structures in Superabsorbing Cellulose Nanofiber Aerogels, J. Phys. Chem. C 123 (2019) 30986–30995.
[44] I. Lazar, I. Fabian, A Continuous Extraction and Pumpless Supercritical CO2 Drying System for Laboratory-Scale Aerogel Production, Gels 2 (2016) 26.
[45] L. Druel, A. Kenkel, V. Baudron, S. Buwalda, T. Budtova, Cellulose Aerogel Microparticles via Emulsion-Coagulation Technique, Biomacromolecules (2020).
[46] G. Beaucage, Approximations leading to a unified exponential power-law approach to small-angle scattering, J. Appl. Crystallogr. 28 (1995) 717–728.
[47] S.M. King, Small-angle neutron scattering, Modern techniques for polymer characterisation, John Wiley & Sons Ltd., Chichester, 1999, pp. 171–232.
[48] S.R. Kline, Reduction and analysis of SANS and USANS data using IGOR Pro, J. Appl. Crystallogr. 39 (2006) 895–900.
[49] S.G. Allen, P.C.L. Stephenson, J.H. Strange, Morphology of porous media studied by nuclear magnetic resonance, J. Chem. Phys. 106 (1997) 7802–7809.
[50] P.J. Barrie, Characterization of porous media using NMR methods, Annu. Rep. NMR Spectr. 41 (2000) 265–316.
[51] M. Simina, R. Nechifor, I. Ardelean, Saturation-dependent nuclear magnetic resonance relaxation of fluids confined inside porous media with micrometer-sized pores, Magn. Reson. Chem. 49 (2011) 314–319.
[52] T. Asakura, K. Isobe, S. Kametani, O.T. Ukpebor, M.C. Silverstein, G.S. Boutis, Characterization of water in hydrated Bombyx mori silk fibroin fiber and films by (2)H NMR relaxation and (13)C solid state NMR, Acta Biomater. 50 (2017) 322–333.
[53] I. Bardenhagen, W. Dreher, D. Fenske, A. Wittstock, M. Bäumer, Fluid distribution and pore wettability of monolithic carbon xerogels measured by 1H NMR relaxation, Carbon 68 (2014) 542–552.
[54] S.G. Allen, P.C.L. Stephenson, J.H. Strange, Internal surfaces of porous media studied by nuclear magnetic resonance cryoporometry, J. Chem. Phys. 108 (1998) 8195–8198.
[55] J.C. Dore, J.B.W. Webber, J.H. Strange, Characterisation of porous solids using small-angle scattering and NMR cryoporometry, Colloid. Surface. A 241 (2004) 191–200.
[56] O.V. Petrov, I. Furo, NMR cryoporometry: Principles, applications and potential, Prog. Nucl. Magn. Res. Spect. 54 (2009) 97–122.
[57] C. Ammann, P. Meier, A. Merbach, A simple multinuclear NMR thermometer, J. Magn. Reson. 46 (1982) (1969) 319–321.
[58] Y. Cohen, L. Avram, L. Frish, Diffusion NMR spectroscopy in supramolecular and combinatorial chemistry: an old parameter–new insights, Angew. Chem. Int. Ed. 44 (2005) 520–554.
[59] C.S. Johnson, Diffusion ordered nuclear magnetic resonance spectroscopy: principles and applications, Prog. Nucl. Mag. Res. Sp. 34 (1999) 203–256.
[60] M. Keri, Z. Nagy, L. Novak, E. Szarvas, L.P. Balogh, I. Banyai, Beware of phosphate: evidence of specific dendrimer-phosphate interactions, Phys. Chem. Chem. Phys. 19 (2017) 11540–11548.
[61] M. Keri, C. Peng, X. Shi, I. Banyai, NMR characterization of PAMAM_G5.NH2 entrapped atomic and molecular assemblies, J. Phys. Chem. B, 119 (2015) 3312-3319.
[62] C.H. Cho, Y.S. Hong, K. Kang, V.I. Volkov, V. Skirda, C.Y. Lee, C.H. Lee, Water self-diffusion in Chlorella sp. studied by pulse field gradient NMR, Magn. Reson. Imaging 21 (2003) 1009–1017.
[63] T.J. Rottreau, C.M.A. Parlett, A.F. Lee, R. Evans, Diffusion NMR Characterization of

Catalytic Silica Supports: A Tortuous Path, J. Phys. Chem. C 121 (2017) 16250–16256.
[64] R. Valiullin, V. Skirda, Time dependent self-diffusion coefficient of molecules in porous media, J. Chem. Phys. 114 (2001) 452–458.
[65] J. Kalmar, M. Keri, Z. Erdei, I. Banyai, I. Lazar, G. Lente, I. Fabian, The pore network and the adsorption characteristics of mesoporous silica aerogel: adsorption kinetics on a timescale of seconds, RSC Adv. 5 (2015) 107237–107246.
[66] M. Thommes, K. Kaneko, A.V. Neimark, J.P. Olivier, F. Rodriguez-Reinoso, J. Rouquerol, K.S.W. Sing, Physisorption of gases, with special reference to the evaluation of surface area and pore size distribution (IUPAC Technical Report), Pure Appl. Chem. 87 (2015) 1051–1069.
[67] C.J. Gommes, A.P. Roberts, Stochastic analysis of capillary condensation in disordered mesopores, Phys. Chem. Chem. Phys. 20 (2018) 13646–13659.
[68] P.W. Schmidt, Small-Angle Scattering Studies of Disordered, Porous and Fractal Systems, J. Appl. Crystallogr. 24 (1991) 414–435.
[69] A.Y. Cherny, E.M. Anitas, V.A. Osipov, A.I. Kuklin, A model of small-angle scattering from three-phase fractal systems, J. Phys. Conf. Ser. 393 (2012).
[70] B. Hammouda, A new Guinier-Porod model, J. Appl. Crystallogr. 43 (2010) 716–719.
[71] K.A.D. Obrey, K.V. Wilson, D.A. Loy, Enhancing mechanical properties of silica aerogels, J. Non-Cryst. Solids 357 (2011) 3435–3441.
[72] K.E. Parmenter, F. Milstein, Mechanical properties of silica aerogels, J. Non-Cryst. Solids 223 (1998) 179–189.
[73] T. Woignier, J. Phalippou, Mechanical Strength of Silica Aerogels, J. Non-Cryst. Solids 100 (1988) 404–408.
[74] G.V. Franks, Zeta potentials and yield stresses of silica suspensions in concentrated monovalent electrolytes: isoelectric point shift and additional attraction, J. Colloid Interface Sci. 249 (2002) 44–51.
[75] H. Che, H. Zhang, Y. Tian, P.F.H. Lai, Y. Xia, S. Wang, L. Ai, Exopolysaccharide from Streptococcus thermophilus as stabilizer in fermented dairy: Binding kinetics and interactions with casein of milk, Int. J. Biol. Macromol. 140 (2019) 1018–1025.
[76] A. Luk, N.S. Murthy, W. Wang, R. Rojas, J. Kohn, Study of nanoscale structures in hydrated biomaterials using small-angle neutron scattering, Acta Biomater. 8 (2012) 1459–1468.
[77] C.I. Merzbacher, J.G. Barker, K.E. Swider, D.R. Rolison, Effect of re-wetting on silica aerogel structure: a SANS study, J. Non-Cryst. Solids 224 (1998) 92–96.
[78] C.G. de Kruif, T. Huppertz, V.S. Urban, A.V. Petukhov, Casein micelles and their internal structure, Adv. Colloid Interface Sci. 171–172 (2012) 36–52.
[79] A. Otsuki, L. de Campo, C.J. Garvey, C. Rehm, H2O/D2O Contrast Variation for Ultra-Small-Angle Neutron Scattering to Minimize Multiple Scattering Effects of Colloidal Particle Suspensions, Colloid Interfac. 2 (2018) 37.
[80] V.M. Gun'ko, V.V. Turov, E.M. Pakhlov, T.V. Krupska, B. Charmas, Effect of water content on the characteristics of hydro-compacted nanosilica, Appl. Surf. Sci. 459 (2018) 171–178.
[81] T.J. Rottreau, G.E. Parkes, M. Schirru, J.L. Harries, M.G. Mesa, P.D. Topham, R. Evans, NMR cryoporometry of polymers: Cross-linking, porosity and the importance of probe liquid, Colloid. Surface. A 575 (2019) 256–263.
[82] J. Wang, H. Xue, B. Zhou, Y.F. Yao, E.W. Hansen, Interfacial water in mesopores and its implications to the surface features – A solid state NMR study, Appl. Surf. Sci. 484 (2019) 1154–1160.
[83] V.M. Gun'ko, Composite materials: Textural characteristics, Appl. Surf. Sci. 307 (2014) 444–454.
[84] N. Gopinathan, B. Yang, J.P. Lowe, K.J. Edler, S.P. Rigby, NMR cryoporometry characterisation studies of the relation between drug release profile and pore structural evolution of polymeric nanoparticles, Int. J. Pharm. 469 (2014) 146–158.
[85] V.M. Gun'ko, V.V. Turov, R. Leboda, V.I. Zarko, J. Skubiszewska-Zieba, B. Charmas, Comparative analysis of heterogeneous solid and soft materials by adsorption, NMR and thermally stimulated depolarisation current methods, Appl. Surf. Sci. 253 (2007) 5640–5644.
[86] B.T. Nguyen, G. Balakrishnan, B. Jacquette, T. Nicolai, C. Chassenieux, C. Schmitt, L. Bovetto, Inhibition and Promotion of Heat-Induced Gelation of Whey Proteins in the Presence of Calcium by Addition of Sodium Caseinate, Biomacromolecules 17 (2016) 3800–3807.
[87] C. Rondeau-Mouro, D. Defer, E. Leboeuf, M. Lahaye, Assessment of cell wall porosity in Arabidopsis thaliana by NMR spectroscopy, Int. J. Biol. Macromol. 42 (2008) 83–92.
[88] P.M. Kekkonen, A. Ylisassi, V.V. Telkki, Absorption of Water in Thermally Modified Pine Wood As Studied by Nuclear Magnetic Resonance, J. Phys. Chem. C 118 (2014) 2146–2153.
[89] J. Götz, R. Hinrichs, Diffusion and relaxation in gels, in: Modern magnetic resonance, Springer, 2008, pp. 1713-1719.
[90] F. Gallego-Gomez, C. Cadar, C. Lopez, I. Ardelean, Microporosity Quantification via NMR Relaxometry, J. Phys. Chem. C 123 (2019) 30486–30491.
[91] F. Gallego-Gomez, C. Cadar, C. Lopez, I. Ardelean, Imbibition and dewetting of silica colloidal crystals: An NMR relaxometry study, J. Colloid Interface Sci. 561 (2020) 741–748.
[92] M.A. Gagnon, M. Lafleur, Comparison of the structure and the transport properties of low-set and high-set curdlan hydrogels, J. Colloid Interface Sci. 357 (2011) 419–427.
[93] F. Elwinger, P. Pourmand, I. Furo, Diffusive Transport in Pores. Tortuosity and Molecular Interaction with the Pore Wall, J. Phys. Chem. C 121 (2017) 13757–13764.
[94] D. Benjamini, J.J. Elsner, M. Zilberman, U. Nevo, Pore size distribution of bioresorbable films using a 3-D diffusion NMR method, Acta Biomater. 10 (2014) 2762–2768.
[95] P.J. Back, A. Coy, Y. Xia, P.T. Callaghan, L.M. Diamante, S.L. Umbach, Some biophysical applications of motional contrast in n.m.r. microscopy, Int. J. Biol. Macromol. 13 (1991) 181–189.
[96] M. Holz, S.R. Heil, A. Sacco, Temperature-dependent self-diffusion coefficients of water and six selected molecular liquids for calibration in accurate 1H NMR PFG measurements, Phys. Chem. Chem. Phys. 2 (2000) 4740–4742.
[97] D. Noferini, A. Faraone, M. Rossi, E. Mamontov, E. Fratini, P. Baglioni, Disentangling Polymer Network and Hydration Water Dynamics in Polyhydroxyethyl Methacrylate Physical and Chemical Hydrogels, J. Phys. Chem. C 123 (2019) 19183–19194.
[98] F. Vaca Chavez, E. Hellstrand, B. Halle, Hydrogen exchange and hydration dynamics in gelatin gels, J. Phys. Chem. B 110 (2006) 21551–21559.
[99] M. Vorob'ev, Bound water measurements for aqueous protein solutions and food gels, Colloid. Surface. B 31 (2003) 133–140.
[100] G. Nystrom, W.K. Fong, R. Mezzenga, Ice-Templated and Cross-Linked Amyloid Fibril Aerogel Scaffolds for Cell Growth, Biomacromolecules 18 (2017) 2858–2865.